Tuning of Intrinsic Magnetic Damping Parameter in Epitaxial CoNi (001) Films: Role of Band Filling Effect

S. J. Xu,[1] J. Y. Shi,[2] Y. S. Hou,[3] Z. Zheng,[2] H. B. Zhao,[2] R. Q. Wu,[3] S. M. Zhou,[1] Z. Shi,[1] and W. J. Fan[1,*]

[1]*Shanghai Key Laboratory of Special Artificial Microstructure Materials and Technology and Pohl Institute of Solid State Physics and School of Physics Science and Engineering, Tongji University, Shanghai 200092, China*

[2]*Shanghai Ultra-precision Optical Engineering Research Center, and Key Laboratory of Micro and Nano Photonic Structures (Ministry of Education), Department of Optical Science and Engineering, Fudan University, Shanghai, 200433, China*

[3]*Department of Physics and Astronomy, University of California, Irvine, California 92697-4575, USA*

(Dated: June 17, 2019)

Band filling effect, which is due to tuning the electron occupation number near the Fermi level, on the intrinsic magnetic damping parameter is demonstrated by employing high quality epitaxial $Co_{1-x}Ni_x$ alloy films, in which the Fermi level and the density of states can be continuously tuned by varying the Ni concentration x. The intrinsic magnetic damping parameter, measured by time-resolved magneto-optical Kerr effect, changes weakly at small x and increases sharply for $x > 0.80$. The experimental results are well reproduced by the density functional theory calculation. More interestingly, the magnetic damping parameter and the density of states near the Fermi level share similar variation trends, demonstrating their correlation. The band filling effect in $3d$ magnetic transition metal alloys provides a way to tune the magnetic damping parameter as a key element in controlling of energy loss and speed of spintronic devices.

PACS numbers: 72.25.Rb, 71.20.Be, 71.70.Ej, 75.78.-n

Introduction

In the design of high-speed information storage technology, the magnetic damping parameter determines the characteristic times of magnetic relaxation of magnetization procession because it strongly affects the required energy and speed of operations[1–3]. Ultra-low magnetic damping is found in insulating ferromagnets such as yttrium-iron-garnet[4–9], and also in metallic ferromagnetic thin films[10–15]. *Ab initio* calculations, based on the breathing Fermi-surface model, generalized torque correlation model, and scattering model, have been performed to reveal the mechanism of the magnetic damping in metallic ferromagnets[16–23]. According to the breathing Fermi-surface model, the magnetic damping parameter is related to both the strength of spin orbital coupling and the density of states (DOS) near the Fermi level[16–18]. Recently, He *et al.*[24] reported the variation of magnetic damping of $Fe_{0.5}(Pd_xPt_{1-x})_{0.5}$ epitaxial alloys with the Pt atomic concentration and explained the phenomena in terms of altering spin-orbit interaction. Low magnetic damping parameters in measurements for $Fe_{25}Co_{75}$ films[10,11] and half-metallic Heusler alloys[14,15] agree with an interesting theoretical finding that the magnetic damping parameter is proportional to the DOS near the Fermi level[16–18]. If this conjecture is confirmed, the magnetic damping parameter can be tuned by adjusting Fermi level with different alloy compositions[10,11,14,15].

It is noted that the phase transition, from body centered cubic (BCC) to face-centered-cubic (FCC), may happen in many alloys such as FeCo as the alloy composition changes[10]. This may complicate studies of damping-composition relation because of the abrupt changes of DOS. CoNi disordered alloy films have single FCC structure and can be easily deposited at all compositions by epitaxial growth[25].Their DOS at the Fermi level can be *continuously* tuned by changing the alloy composition. Hence, CoNi alloys are ideal to investigating the band filling effect on magnetic damping, through changing the Fermi level as a function of the alloy composition.

In order to elucidate the mechanism of the intrinsic magnetic damping α_0, we have fabricated high quality epitaxial $Co_{1-x}Ni_x$ (=CoNi) disordered alloy films on $SrTiO_3$ (STO)(100) substrates. Since Co and Ni metals have different *3d* electrons, the Fermi level and thus the DOS of CoNi alloys can be continuously and significantly tuned by the alloy composition. The electronic structure calculations have been performed based on density functional theory (DFT). The time-resolved magneto-optical Kerr effect (TRMOKE) measurements show strong dependence of the magnetic damping on the Ni chemical concentration x. The experimental results are well reproduced by DFT calculations. The magnetic damping and the DOS at Fermi level show similar variation trends as a function of x for the $3d$ magnetic transition metal alloys.

Experiments

A series of 20 nm thick $Co_{1-x}Ni_x$ disordered alloy films were deposited from CoNi ($0 \leq x \leq 1.0$) alloy targets on STO (001) single crystalline substrates

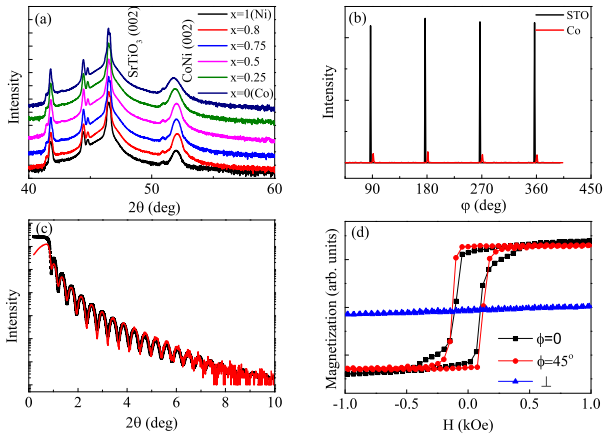

FIG. 1: (a) XRD spectra of $Co_{1-x}Ni_x$ thin films on STO substrates. (b) φ scanning at $2\theta = 44.36°$ for the Co film and $2\theta = 39.98°$ for the STO substrate. (c) Measured XRR (black line) and fitting curve (red line) of a typical Co sample. (d) Hysteresis loops of Co film with the external magnetic field along [100], [110] and [001] orientations.

by high vacuum DC magnetron sputtering with a base pressure lower than 3×10^{-5} Pa and a working Ar pressure at 0.35 Pa. The deposition rate is 0.1 nm/s. STO substrates were kept at 650°C for 1 hour to remove the surface contamination and were then cooled to 500°C before deposition. The substrates were kept at 500°C during deposition and for another 2 hours after deposition to get high quality single crystalline structure. The microstructure of all samples and the thickness and the surface roughness were characterized by x-ray diffraction (XRD) and x-ray reflectivity (XRR), respectively, with a Bruker D8 diffractometer with 5-axis configuration and Cu Kα ($\lambda = 0.1542$ nm). The planar Hall effect (PHE) was measured by physical properties measurement system (PPMS) with standard Hall bar patterns. Magnetization hysteresis loops were measured by vibrating sample magnetometry. Measurements of Gilbert damping were performed by TRMOKE. We used 400-nm laser pulses of 1 kHz repetition rate for the pump beam, which was focused on the sample at the fluence of 0.4 mJ/cm^2. The 400-nm pulses were generated by frequency doubling of 800-nm pulses (100 fs) using a beta barium borate (BBO) crystal. The transient MOKE signal was detected by a much weaker probe beam of 800 nm at an incident angle of 45° in a balanced detection mode. A vector magnet was used to provide magnetic field along arbitrary directions in the sample plane. All measurements in the present work were performed at room temperature.

Results and discussion

Figure 1(a) shows the XRD spectra of CoNi alloys for $0 \leq x \leq 1$, two peaks are found near 46° and 52°, corresponding to FCC STO 002 and CoNi 002 diffractions, respectively. Since no diffraction peaks for $L1_0$ and $L1_2$ structures are observed in XRD spectra, all samples were chemically disordered. This coincides with the results that the sheet resistivity achieves a maximal value near $x = 0.75$ (not shown), indicating the random locations of Ni and Co atoms[26,27]. The lattice constant along the film normal direction is 0.352 nm for all samples. Moreover, the diffraction peak of (111) plane is located at $2\theta = 44.36°$ and accordingly the in-plane lattice constant is also 0.352 nm. Therefore, there is no lattice distortion in the present CoNi films, due to the lattice relaxation. Figure 1(b) shows the φ scanning at $2\theta = 44.36°$ for Co and $2\theta = 39.98°$ for STO substrate. The Co film and STO substrate have the same four-fold symmetry, and prove the epitaxial growth of the samples. The results in Figs. 1(a) and 1(b) indicate that all CoNi films are of FCC structure. The thickness and the surface roughness are fitted from XRR spectra (in Fig. 1 (c)) to be close to the designed value of 20.0 nm and to be about 0.2 nm for Co films, respectively. For all samples, the interference fringes can be observed in a wide angle region from the critical angle, $2\theta \approx 1.0$ degree, to 8.00 degrees, indicating low surface roughness. In-plane magnetic hysteresis loops of Co sample are shown in Fig. 1(d), the external magnetic fields are applied at 0° and 45° to the [100] axis, respectively. From the hysteresis loops, we can get coercive field at 130 Oe for easy axis and 100 Oe for hard axis. The slanted out-of plane hysteresis loop shows the in-plane magnetic anisotropy in the present systems. In a word, epitaxially grown CoNi alloy films with high quality are achieved in the present work.

The magnetocrystalline and the uniaxial magnetic anisotropy parameters K_1 and K_u are measured by Planer Hall Effect (PHE), where PHE voltage is proportional to $2\sin\phi\cos\phi$. The schematic picture of PHE measurements is shown in Fig. 2(a). The magnetization may advance or lag behind the magnetic field H and they coincide with each other at $\phi_H = 0$, 90, 180, and 270 (degrees), as shown in Fig. 2 (b). From a PHE curve as a function of ϕ_H, the values of ϕ and $\phi - \phi_H$ can be deduced, where ϕ and ϕ_H are the in-pane angles of the magnetization and the applied field with respect to the [010] orientation, respectively. Therefore, a typical torque curve (Fig. 2(c)) can be gained by calculating $L = M_S H \sin(\phi - \phi_H)$, where M_S is the saturated magnetization and H is the applied field. According to the equilibrium equation $\partial E/\partial\phi = 0$, where the free energy consists of the magnetic crystalline anisotropy energy, the uniaxial anisotropy energy, and the Zeeman energy, i.e., $E = E_Z + E_K$, $E_Z = -M_S H\cos(\phi_H - \phi)$, and

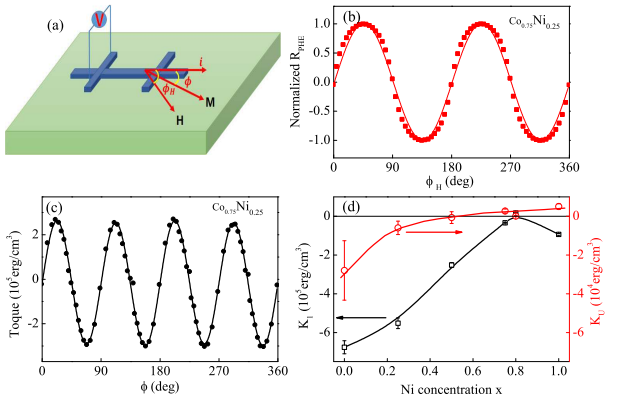

FIG. 2: (a) Schematic geometry of PHE measurements. (b) PHE curve of typical $Co_{0.75}Ni_{0.25}$ film at $H = 2.0$ kOe. (c) Torque curve of $Co_{0.75}Ni_{0.25}$ film as a function of ϕ. (d) K_1 and K_u with varying Ni concentration x. Solid lines refer to $\sin(2\phi_H)$ in (b) and $L = K_1 \sin 4\phi + K_u \sin 2\phi$ in (c) fitted results, and serve a guide to the eye in (d).

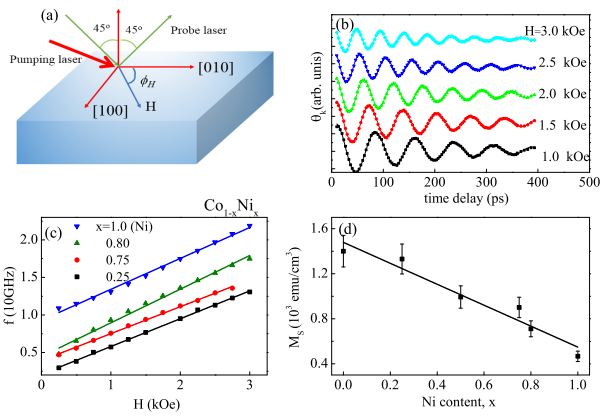

FIG. 3: Schematic geometry of TRMOKE measurements (a). Measured TRMOKE results for the $Co_{0.75}Ni_{0.25}$ film under different in-plane external magnetic field at $\phi_H = 75$ degrees with respect to [010](b). Precession frequency f versus H for different samples (c) and saturation magnetization M_S as a function of x (d).

$E_K = K_1 \sin^2\phi\cos^2\phi + K_u \sin^2\phi$ with the magnetization aligned in the film plane. Thus, one also has $L = K_1 \sin 4\phi + K_u \sin 2\phi$. The magnetic torque curves are fitted and the magnetocrystalline anisotropy K_1 and the uniaxial magnetic anisotropy K_u (the demagnetization energy not included) can be determined for all samples, as shown in Fig. 2(d). The magnetocrystalline anisotropy K_1 approaches zero near $x = 0.8$ and is negative for other samples[25]. In particular, it is interesting to find that K_1 is almost zero near $x = 0.80$ although it is negative K_1 for both FCC Co and Ni. Similar phenomena were observed in epitaxial NiFe films[28]. The peculiar nonmonotonic variation of the magnetocrystalline anisotropy with the alloy composition is attributed to the band filling effect when the Fermi level is shifted with the alloy composition. Meanwhile, K_u is found to be more than 10 times smaller than K_1 in magnitude and to decrease monotonously with the increasing Ni concentration x of $Co_{1-x}Ni_x$. Therefore, the attribute of soft magnet can be understood near $x = 0.80$. With negative K_1 and negligible K_u, the cubic edges $\langle 100\rangle$ is the hard directions and $\langle 110\rangle$ are the medium hard directions[29], in coincide with the results of Fig. 1(d).

The magnetization precession relaxation time is measured by the TRMOKE. A variable magnetic field up to 3.0 kOe was applied at 75° to the [010] orientation of the sample as shown in Fig. 3(a). The TRMOKE results of the $Co_{0.75}Ni_{0.25}$ film under different magnetic fields are shown in Fig. 3(b). The magnetic damping is demonstrated by the decay of the magnetization precession with the time delay. The MOKE signal can be fitted by $\theta_k = a + A\exp(-t/\tau_s)\sin(2\pi f t + \phi_0)$, where f is the precession frequency and τ_s is the spin precession relaxation time, A is the amplitude, ϕ_0 is the phase of the magnetization precession, and the parameter a corresponds to the background signal. It is found that the precession frequency increases with increasing H. Figure 3(c) shows the dispersion relationship, i.e., frequency f versus the external magnetic field H for different samples. The dispersion can be fitted by the following Kittel equation[30],

$$
\begin{aligned}
f &= \gamma(H_1 H_2)^{1/2} \\
H_1 &= 4\pi M_s - \frac{2K_u}{M_s}\sin^2\phi + \frac{2K_1}{M_s}(2 - \sin^2 2\phi) \\
&\quad + H\cos(\phi - \phi_H) \\
H_2 &= \frac{2K_u}{M_s}\cos^2\phi + \frac{2K_1}{M_s}\cos 4\phi \\
&\quad + H\cos(\phi - \phi_H),
\end{aligned}
\tag{1}
$$

where γ is the gyromagnetic ratio and ϕ can be obtained by the equilibrium equation $\partial E/\partial\phi = 0$. With the data of K_1 and K_u in Fig. 2(d), and of the saturation magnetization M_S in Fig. 3(d) for all samples, the gyromagnetic ratio γ is calculated to be 2.01, 2.068, 2.10, 1.913, 1.80, and 1.91 (10^7 $s^{-1}Oe^{-1}$), and the g factor is 2.27, 2.34, 2.37, 2.16, 2.03, and 2.16 for $x = 0$ (Co), 0.25, 0.50, 0.75, 0.80, and 1.0 (Ni), respectively. The values of g are close to the results of literatures[31,32]. The non-vanishing $g - 2.0$ term indicates the effect of the spin orbital interaction in CoNi alloys[17]. Here, M_S of the CoNi alloys, measured by VSM, is plotted as a function of Ni concentration x. The variation trend obeys the Slater-Pauling curve[31].

The damping parameter α can be determined by fitting the following H dependent precession relaxation

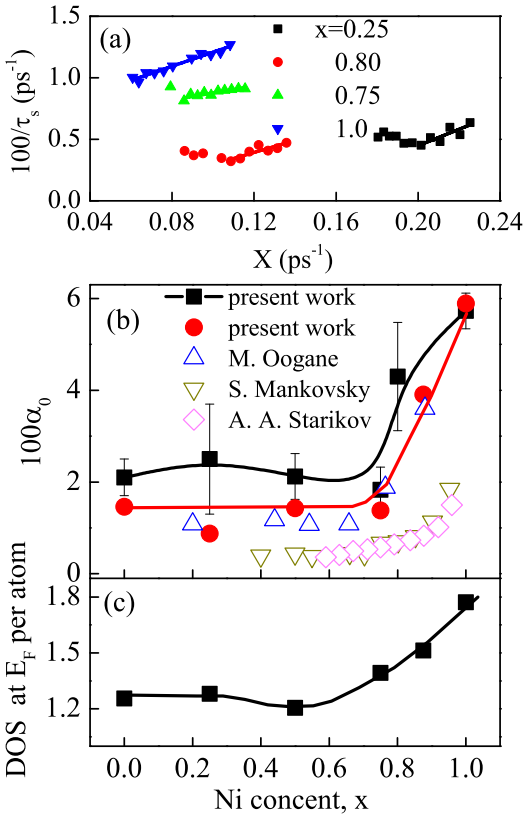

FIG. 4: Relaxation rate $1/\tau_s$ versus the term X for $x = 0.25$, 0.75, 0.80, and 1.0, where $X = \gamma(H_1 + H_2)/2$ (a), measured (black squares) and DFT calculated (red circles) magnetic damping parameter α_0 (b) and DOS at Fermi level (c) as a function of x. In comparison, experimental data of M. Oogane *et al.* (uptriangles)[12], calculated results of S. Mankovsky *et al.*(downtriangles)[13] and A. A. Starikov *et al.*(diamonds)[21] are also given in (b). The solid lines refer to the linear fitting results in (a) and serve to the eye in (b, c).

rate[33],

$$1/\tau_s = \alpha\gamma(H_1 + H_2)/2 = \alpha X$$
$$X = \gamma(H_1 + H_2)/2. \quad (2)$$

where H_1 and H_2 are defined in Eq. 1. Figure 4(a) presents a plot of $1/\tau_s$ versus X. Apparently, $1/\tau_s$ changes linearly as a function of X for $x = 0.25$, 0.75, 0.80, and 1.0 at high H whereas the data at lower H may deviate from the linear dependence because the samples are not saturated[11]. The slope corresponds to the intrinsic magnetic parameter α_0 whereas the intercept is caused by the extrinsic contribution to the entire magnetic damping. The intrinsic one is related to the electronic band structure near the Fermi level. Since the extrinsic one is caused by microstructural inhomogeneity and depends on the magnitude of the external magnetic field, the linear dependence can be obtained only when the extrinsic one is almost suppressed under strong external magnetic fields[34]. In the following, we will focus on the intrinsic one α_0. Figure 4(b) shows that the measured intrinsic magnetic damping parameter α_0 almost keeps constant for small x and varies significantly for $x > 0.80$. The value of α_0 at small x is three times less than the maximum value of pure Ni sample. Since the spin precession relaxation time τ_s depends on the term X, it changes significantly with both the alloy composition and the magnitude of the external magnetic field, as shown in Fig. 4(a).

DFT calculations are carried out with Vienna *ab initio* Simulation Package (VASP)[35,36]. We use the experimentally measured lattice constants and special quasi-random structures (SQSs) of 32 atoms[37,38] for $Co_{1-x}Ni_x$ alloys. To calculate the intrinsic damping α_0, we utilize our recently extended torque method[39] that is based on the scattering theory of the magnetic damping[40]. Note that the scattering theory of Gilbert damping and the Kamberskys torque-correlation model have the same essential physics in damping, since both capture the intraband (conductivity-like) and interband (resistivity-like) contributions. The measured results are reproduced by the calculations, that is to say, both of the experimental and calculated damping parameter α_0 change weakly from $x = 0$ to $x = 0.80$, and then they significantly increase and have a maximum for pure Ni, as shown in Fig. 4(b). Figure 4(c) is the DFT calculated DOS at the Fermi energy for $Co_{1-x}Ni_x$ alloys, where the Fermi energy is 5.42, 5.36, 5.21, 5.02, 4.92, 4.78 (eV) for $x = 0$, 0.25, 0.50, 0.75, 0.875, and 1.0, respectively. It is found that the DOS at the Fermi level and the damping parameter α_0 have similar trends. This is consistent with the breathing Fermi-surface model[22]. In addition to the Fermi energy, the electronic band structure near the Fermi level is expected to change gradually with x, as demonstrated by different DOS distributions near the Fermi level for various x in Fig. 5. Accordingly, the change of DOS near the Fermi level in Fig. 4(c) is induced by the alternations of both electronic band structure and Fermi energy level shift.

It is essential to analyze effects of other factors, such as, the relaxation time of electronic momentum and the shape of the Fermi surface, on the intrinsic magnetic damping parameters of CoNi alloys. The intrinsic magnetic damping parameter of epitaxial CoNi films is larger than that of polycrystalline ones, as shown in Fig. 4(b), although the intrinsic magnetic damping parameter shows similar variation trends with x for both polycrystalline and single crystalline CoNi films. Similar phenomena have also been observed in polycrystalline and epitaxial FeCo films[10,11]. The difference of the intrinsic magnetic damping parameter between single and polycrystalline films can be explained in terms of the

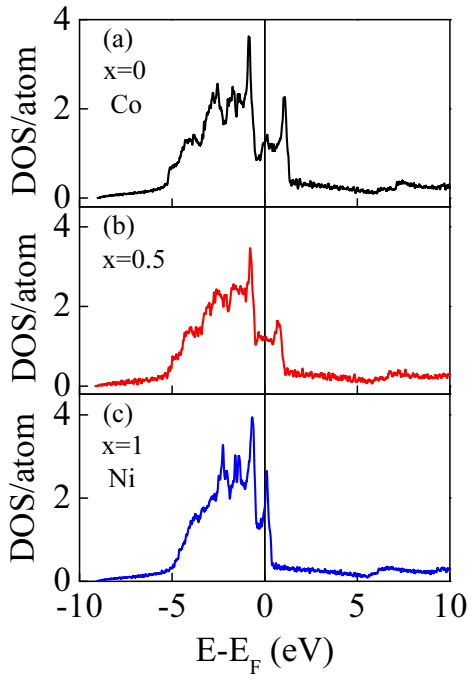

FIG. 5: DOS per atom versus the energy for $x = 0$(a), 0.50 (b), and 1.0 (c). Here, the Fermi energy is 5.42, 5.21, and 4.78 (eV) for $x = 0$, 0.50, and 1.0, respectively.

anisotropy of the Fermi surface and the relaxation time of electronic momentum. First, the intrinsic magnetic damping parameter strongly depends on the shape of the Fermi surface and exhibits anisotropy[41], leading to the difference between single and polycrystalline CoNi films. Secondly, the intrinsic magnetic damping parameter strongly depends on the relaxation time of electronic momentum which is in turn related to the microstrucutre of CoNi films. With the dominant contribution of the intraband transition, for example, the magnetic damping parameter is proportional to the relaxation time of electronic momentum[17,22,23], and it increases sharply for longer relaxation time of electronic momentum. For high quality epitaxial films, the relaxation time of electronic momentum is expected to be longer than that of the intrinsic polycrystalline films, due to different defect distributions and short range order of atoms[26]. Accordingly, larger magnetic damping parameters are achieved in epitaxial films. Very recently, the anisotropy of magnetic damping has been observed experimentally in epitaxial films of Fe on GaAs(001) substrates and FeCo on MgO(001) substrates[41,43]. The anisotropy of magnetic damping is ascribed to the crystal orientation-dependent density of states near the Fermi surface in Fe/GaAs and to the anisotropy of spin orbit coupling strength in CoFe/MgO. In the present experiments, therefore, the value of the (intrinsic) magnetic damping depends on the orientation of the external magnetic field with respect to the crystal orientation. In contrast, for polycrystalline films, the crystal orientations of all small crystals are aligned randomly, leading to an average effect on the magnetic damping. Again, with a closer look at the results in Fig. 4(b), one can find that the calculated value of the intrinsic magnetic damping parameter is equal to the measured one at $x = 1.0$ whereas it is slightly smaller than that of the measured value at $x < 1.0$. This phenomenon can be ascribed to the artifact that the relaxation time of electronic momentum also changes with the alloy composition[16–19]. Interestingly, the intrinsic magnetic damping parameter in epitaxially grown Co/Ni multilayers with perpendicular magnetic anisotropy is smaller than that of polycrystalline samples, due to the alternative stacking of ultrathin Co and Ni layers, different from the present results[42]. Finally, the disagreement between the experimental and the previous calculation results is mainly due to the vertex corrections used in the first principle calculation in Ref.13, which accounts into the angular-momentum transfer between the precessing magnetization and the itinerant carriers. Since the vertex corrections will lead to underestimation of the intrinsic magnetic damping parameter, our results are slightly larger than the numerical results of Mankovsky and Starikov *et al.*[13,21].

In short summary, a series of high quality epitaxial $Co_{1-x}Ni_x$ disordered alloy films were grown on STO (100) substrates. The Fermi level can be continuously tuned by changing the alloy composition. The intrinsic damping parameter α_0, measured by TRMOKE, does not change much for $x < 0.80$ and increases sharply for $x > 0.80$. The experimental results of α_0 are well reproduced by the DFT calculations. Particularly, the band filling effect is demonstrated by similar variation trends of the intrinsic magnetic damping parameter and the DOS at the Fermi level, as a function of the chemical concentration of Ni. This very effect arises from the combination of the electronic band structure and the Fermi energy with the varying Ni content x. Moreover, the intrinsic magnetic damping parameter is also found to strongly depend on the relaxation time of electronic momentum through varying microstructure.

This work was supported by the State Key Project of Fundamental Research Grant No.2015CB921501, National Key R & D Program of China Grand No. 2017YFA0305300 and 2017YFA0303202, the National Science Foundation of China Grant Nos.51501131, 51671147, 11874283, 11674246, and 11774259, Shanghai Committee of Science and Technology under grant No.17ZR1443700 and 17142202300, and the Fundamental Research Funds for the Central Universities. Work at University of California, Irvine

was supported by DOE-BES (grant no. DE-FG02-05ER46237), and the computer simulations were supported by the National Energy Research Scientific Computing Center (NERSC).

* Electronic address: fanwj@tongji.edu.cn

[1] I. Žutić, J. Fabian, and S. DasSarma, Rev. Mod. Phys. **76**, 323410 (2004)

[2] S. Emori, U. Bauer, S.-M. Ahn, E. Martinez, and G. S. D. Beach, Nat. Mater. **12**, 611616 (2013)

[3] E. Jué, C. K. Safeer, M. Drouard, A. Lopez, P. Balint, L. Buda-Prejbeanu, O. Boulle, S. Auffret, A. Schuhl, A. Manchon, I. M. Miron, and G. Gaudin, Nat. Mater. **15**, 272277 (2016)

[4] Y. Y. Sun, H. Chang, M. Kabatek, Y.-Y. Song, Z. Wang, M. Jantz, W. Schneider, M. Wu, E. Montoya, B. Kardasz, B. Heinrich, S. G. E. te Velthuis, H. Schultheiss, and A. Hoffmann, Phys. Rev. Lett. **111**, 106601 (2013)

[5] A. A. Serga, A. V. Chumak, and B. Hillebrands, J. Phys. D **43**, 264002 (2010)

[6] O. d'Allivy Kelly, A. Anane, R. Bernard, J. Ben Youssef, C. Hahn, A. H. Molpeceres, C. Carret ero, E. Jacquet, C. Deranlot, P. Bortolotti, R. Lebourgeois, J.-C. Mage, G. de Loubens, O. Klein, V. Cros, and A. Fert, Appl. Phys. Lett. **103**, 082408 (2013)

[7] J. T. Brangham, K.-Y. Meng, A. S. Yang, J. C. Gallagher, B. D. Esser, S. P. White, S. Yu, D. W. McComb, P. C. Hammel, and F. Y. Yang, Phys. Rev. B **94**, 054418 (2016)

[8] B. Heinrich, C. Burrowes, E. Montoya, B. Kardasz, E. Girt, Y. Y. Song, Y. Y. Sun, and M. Z. Wu, Phys. Rev. Lett. **107**, 066604 (2011)

[9] D. Meier, D. Reinhardt, M. van Straaten, C. Klewe, M. Althammer, M. Schreier, S. T. B. Goennenwein, A. Gupta, M. Schmid, C. H. Back, J.-M. Schmalhorst, T. Kuschel, and G. Reiss, Nat. Commun. **6**, 8211 (2015)

[10] M. A. W. Schoen, D. Thonig, M. L. Schneider, T. J. Silva, H. T. Nembach, O. Eriksson, O. Karis, and J. M. Shaw, Nat. Phys. **12**, 839 (2016)

[11] A. J. Lee, J. T. Brangham, Y. Cheng, S. P. White, W. T. Ruane, B. D. Esser, D. W. McComb, P. C. Hammel, and F. Y. Yang, Nat. Comm. **8**, 234 (2017)

[12] M. Oogane, T. Wakitani, S. Yakata, R. Yilgin, Y. Ando, A. Sakuma, and T. Miyazaki, Jpn J. Appl. Phys. **45**, 3889(2006)

[13] S. Mankovsky, D. Ködderitzsch, G. Woltersdorf, and H. Ebert, Phys. Rev. B **87**, 014430 (2013)

[14] S. Mizukami, D. Watanabe, M. Oogane, Y. Ando, Y. Miura, M. Shirai, and T. Miyazaki, J. Appl. Phys. **105**, 07D306 (2009)

[15] T. Kubota, S. Tsunegi, M. Oogane, S. Mizukami, T. Miyazaki, H. Naganuma, and Y. Ando, Appl. Phys. Lett. **94**, 122504 (2009)

[16] V. Kambersý, Czech. J. Phys. B **34**, 1111 (1984)

[17] V. Kamberský, Czech. J. Phys. B **26**, 1366 (1976)

[18] V. Kamberský, and C. E. Patton, Phys. Rev. B **11**, 2668 (1975)

[19] K. Gilmore, Y. U. Idzerda, and M. D. Stiles, Phys. Rev. Lett. **99**, 027204 (2007)

[20] A. Brataas, Y. Tserkovnyak, and G. E. W. Bauer, Phys. Rev. Lett. **101**, 037207 (2008)

[21] A. A. Starikov, P. J. Kelly, A. Brataas, Y. Tserkovnyak, and G. E. W. Bauer, Phys. Rev. Lett. **105**, 236601 (2010)

[22] K. Gilmore, Y. U. Idzerda, and M. D. Stiles, J. Appl. Phys. **103**, 07D303 (2008)

[23] V. Kamberský, Phys. Rev. B **76**, 134416(2007)

[24] P. He, X. Ma, J. W. Zhang, H. B. Zhao, G. Lüpke, Z. Shi, and S. M. Zhou, Phys. Rev. Lett. **110**, 077203 (2013)

[25] W. J. Fan, L. Ma, Z. Shi, and S. M. Zhou, Chin. Phys. B **24**, 037507 (2015)

[26] L. Nordheim, Ann. Phys. **9**, 664 (1931)

[27] *see*, T. R. Mcguire and R. I. Potter, IEEE Trans. Magn. **11**, 1018(1975)

[28] L. F. Yin, D. H. Wei, N. Lei, L. H. Zhou, C. S. Tian, G. S. Dong, X. F. Jin, L. P. Guo, Q. J. Jia, and R. Q. Wu, Phys. Rev. Lett. **97**, 067203 (2006)

[29] W. X. Tang, D. Qian, D. Wu, Y. Z. Wu, G. S. Dong, X. F. Jin, S. M. Chen, X. M. Jiang, X. X. Zhang, and Z. Zhang, J. Magn. Magn. Mater. **240**, 404 (2002)

[30] C. Kittel, Phys. Rev., **73**, 155(1948)

[31] S. Chikazumi, Physics of Ferromagnetism (Oxford Science, Oxford, 1997)

[32] N. Inaba, H. Asanuma, S. Igarashi, S. Mori, F. Kirino, K. Koike, and H. Morita, IEEE Trans. Magn. **42**, 2372(2006)

[33] C. E. Patton, J. Appl. Phys. 39, 3060 (1968)

[34] W. Zhang, W. He, X. Q. Zhang, Z. H. Cheng, J. Teng, and M. Fähnle, Phys. Rev. B **96**, 220415(2017)

[35] G. Kresse and J. Furthmüller, Phys. Rev. B **54**, 11169 (1996)

[36] G. Kresse and J. Furthmüller, Comp. Mater. Sci. **6**, 15 (1996)

[37] A. Zunger, S. H. Wei, L. G. Ferreira, and J. E. Bernard, Phys. Rev. Lett. **65**, 353 (1990)

[38] J. von Pezold, A. Dick, M. Friák, and J. Neugebauer, Phys. Rev. B **81**, 094203 (2010)

[39] Y. S. Hou and R. Q. Wu, unpublished.

[40] A. Brataas, Y. Tserkovnyak, and G. E. W. Bauer, Phys. Rev. Lett. **101**, 037207 (2008)

[41] Y. Li, F. L. Zeng, S. S.-L. Zhang, H. Shin, H. Saglam, V. Karakas, O. Ozatay, J. E. Pearson, O. G. Heinonen, Y. Z. Wu, A. Hoffmann, and W. Zhang, Phys. Rev. Lett. **122**, 117203 (2019)

[42] T. Seki, J. Shimada, S. Iihama, M. Tsujikawa, T. Koganezawa, A. Shioda, T. Tashiro, W. N. Zhou, S. Mizukami, M. Shirai, and K. Takanashi, J. Phys. Soc. Jpn. **86**, 074710 (2017)

[43] L. Chen, S. Mankovsky, S. Wimmer, M. A. W. Schoen, H. S. Korner, M. Kronseder, D. Schuh, D. Bougeard, H. Ebert, D. Weiss and C. H. Back, Nat. Phys. **14** 490 (2018).